voice leadings. Traditional tonal music exploits this possibility (Fig. 1, A to C, and movie S4). This central feature of Western counterpoint is made possible by composers' interest in the harmonic property of acoustic consonance.

A chord with duplicate pitch classes is permutationally symmetrical (P-symmetrical) because there is some nontrivial permutation of its notes that is a trivial voice leading. These chords lie on the singular boundaries of the orbifolds. Nearly P-symmetrical chords, such as {E, F, G♭}, are near these chords and contain several notes that are clustered close together. Efficient voice leadings permuting the clustered notes bounce off the nearby boundaries (Fig. 2 and movies S2 and S4). Such voice leadings can be independent and nontrivial. Trivial voice leadings are musically inert; therefore, as with T-symmetry, composers have reason to prefer near P-symmetry to exact P-symmetry.

Nearly P-symmetrical chords such as {B, C, D♭} are considered to be extremely dissonant. They are well-suited to static music in which voices move by small distances within an unchanging harmony (Fig. 1D). Such practices are characteristic of recent atonal composition, particularly the music of Ligeti and Lutoslawski. From the present perspective, these avant-garde techniques are closely related to those of traditional tonality: They exploit one of three fundamental symmetries permitting efficient, independent voice leading between transpositionally or inversionally related chords.

A chord is inversionally symmetrical (I-symmetrical) if it is invariant under reflection in pitch-class space. Nearly I-symmetrical chords are near these chords and can be found throughout the orbifolds (16). For example, the F♯ half-diminished seventh chord {6, 9, 0, 4} and the F dominant seventh chord {5, 9, 0, 3} are related by inversion and are very close to the I-symmetrical chord {5.5, 9, 0, 3.5}. Consequently, we can find an efficient voice leading between them, (6, 9, 0, 4) → (5, 9, 0, 3) (Fig. 1C) (16). Nearly T-symmetrical chords, such as the C major triad, and nearly P-symmetrical chords, such as {C, D♭, E♭}, can also be nearly I-symmetrical. Consequently, I-symmetry is exploited in both tonal and atonal music. It plays a salient role in the 19th century, particularly in the music of Schubert (22), Wagner (23), and Debussy (Fig. 1C).

The preceding ideas can be extended in several directions. First, one might examine in detail how composers have exploited the geometry of musical chords. Second, one could generalize the geometrical approach by considering quotient spaces that identify transpositionally and inversionally related chords (24). Third, because cyclical rhythmic patterns can also be modeled as points on $\mathbb{T}^n/\mathcal{S}_n$, one could use these spaces to study African and other non-Western rhythms. Fourth, one could investigate how distances in the orbifolds relate to perceptual judgments of chord similarity. Finally, understanding the relation between harmony and counterpoint may suggest new techniques to contemporary composers.

References and Notes

1. C. Masson, *Nouveau Traité des Règles pour la Composition de la Musique* (Da Capo, New York, 1967).
2. O. Hostinský, *Die Lehre von den musikalischen Klängen* (H. Dominicus, Prague, 1879).
3. D. Huron, *Mus. Percept.* **19**, 1 (2001).
4. J. D. Heinichen, *Der General-Bass in der Composition* (G. Olms, New York, 1969).
5. R. Cohn, *J. Mus. Theory* **41**, 1 (1997).
6. J. Roeder, thesis, Yale University (1984).
7. E. Agmon, *Musikometrica* **3**, 15 (1991).
8. R. Cohn, *Mus. Anal.* **15**, 9 (1996).
9. C. Callender, *Mus. Theory Online* **10** (2004) (http://mto.societymusictheory.org/issues/mto.04.10.3/mto.04.10.3.callender.pdf).
10. G. Mazzola, *The Topos of Music* (Birkhäuser, Boston, 2002).
11. R. Morris, *Mus. Theory Spectrum* **20**, 175 (1998).
12. J. Douthett, P. Steinbach, *J. Mus. Theory* **42**, 241 (1998).
13. J. Straus, *Mus. Theory Spectrum* **25**, 305 (2003).
14. F. Attneave, R. Olson, *Am. Psychol.* **84**, 147 (1971).
15. R. Shepard, *Psychol. Rev.* **89**, 305 (1982).
16. See supporting material on *Science* Online.
17. I. Satake, *Proc. Natl. Acad. Sci. U.S.A.* **42**, 359 (1956).
18. W. Thurston, *The Geometry and Topology of Three-Manifolds* (www.msri.org/publications/books/gt3m).
19. ChordGeometries 1.1 (http://music.princeton.edu/~dmitri/ChordGeometries.html).
20. R. Cohn, *J. Mus. Theory* **35**, 1 (1991).
21. W. Sethares, *Tuning, Timbre, Spectrum, Scale* (Springer, New York, 2005).
22. R. Cohn, *19th Cent. Mus.* **22**, 213 (1999).
23. B. Boretz, *Perspect. New Mus.* **11**, 146 (1972).
24. C. Callender, I. Quinn, D. Tymoczko, paper presented at the John Clough Memorial Conference, University of Chicago, 9 July 2005.
25. Thanks to D. Biss, C. Callender, E. Camp, K. Easwaran, N. Elkies, P. Godfrey Smith, R. Hall, A. Healy, I. Quinn, N. Weiner, and M. Weisberg.

A High-Brightness Source of Narrowband, Identical-Photon Pairs

James K. Thompson,[1]* Jonathan Simon,[2] Huanqian Loh,[1] Vladan Vuletić[1]

We generated narrowband pairs of nearly identical photons at a rate of 5×10^4 pairs per second from a laser-cooled atomic ensemble inside an optical cavity. A two-photon interference experiment demonstrated that the photons could be made 90% indistinguishable, a key requirement for quantum information-processing protocols. Used as a conditional single-photon source, the system operated near the fundamental limits on recovery efficiency (57%), Fourier transform–limited bandwidth, and pair-generation-rate–limited suppression of two-photon events (factor of 33 below the Poisson limit). Each photon had a spectral width of 1.1 megahertz, ideal for interacting with atomic ensembles that form the basis of proposed quantum memories and logic.

The generation of photon pairs is useful for a broad range of applications, from the fundamental [exclusion of hidden-variable formulations of quantum mechanics (1)] to the more practical [quantum cryptography (2) and quantum computation (3)]. A key parameter determining the usefulness of a particular source is its brightness, i.e., how many photon pairs per second are generated into a particular electromagnetic mode and frequency bandwidth. Parametric down-converters based on nonlinear crystals are excellent sources of photon pairs, but they are comparatively dim because their photon bandwidths range up to hundreds of GHz. However, new applications are emerging that demand large pair-generation rates into the narrow bandwidths (5 MHz) suitable for strong interaction of the photons with atoms and molecules (2, 4–7).

We report the development of a source of photon pairs with spectral brightness near fundamental physical limitations and approximately three orders of magnitude greater than the best current devices based on nonlinear crystals (8). Unlike parametric downconverters, however, the atomic ensemble can additionally act as a quantum memory and store the second photon, allowing triggered (i.e., deterministic) generation of the second photon. Triggered delays of up to 20 μs have been demonstrated (9–15), and it is expected that optical lattices hold the potential to extend the lifetime of these quantum memories to seconds (9). Lastly, proposed applications in quantum information (2, 3) rely on joint measurements of single photons for which indistinguishability is crucial for high fidelity. We observe large degrees of indistinguishability in the time-resolved interference between the two generated photons (16–19).

[1]Department of Physics, MIT–Harvard Center for Ultracold Atoms, Research Laboratory of Electronics, Massachusetts Institute of Technology, 77 Massachusetts Avenue, Cambridge, MA 02139, USA. [2]Department of Physics, MIT–Harvard Center for Ultracold Atoms, Harvard University, 17 Oxford Street, Cambridge, MA 02138, USA.

*To whom correspondence should be addressed. E-mail: jkthomps@mit.edu

A range of approaches using atomic ensembles to strongly couple matter and light are actively being pursued. These include room-temperature atomic vapors (10, 11) and laser-cooled atomic ensembles both in free space (12–15) and in optical cavities (9). Simultaneous generation of pairs of strongly correlated photons has been reported (20) with a 7% success rate for generation of the second photon and large violations of a Cauchy-Schwartz inequality (21), $G = 400 > 1$, that indicates the quantum nature of the observed correlations. Three- to fivefold suppressions of undesired two-photon events have been reported (22–24). Single photons have been captured in and released from atomic ensembles (22, 24). Measurement-induced entanglement of independent ensembles of atoms has been demonstrated (23, 25). The two-photon Hong-Ou-Mandel interference used here (16) has also been used to demonstrate the degree of indistinguishability of single photons emitted from quantum dots (17), and from a single atom in a high-finesse cavity (18, 19).

We concentrate on the regime of minimum delay time between the generation of the photons within a pair in order to characterize the source, while keeping in mind that the present results should straightforwardly extend to the regime of delayed photon generation explored in previous work (9). The experimental setup consisted of a laser-cooled ensemble of $N = 10^4$ Cs atoms in the TEM_{00} mode of a low-finesse $F = 250$, single-mode optical cavity (Fig. 1 and supporting online text). Photon pairs were generated by a four-wave mixing process that relies on quantum interference in the emission from an entangled atomic ensemble (2) to enhance the probability of scattering a second "read" photon into the cavity to near unity given the initial scattering of a "write" photon into the cavity (Fig. 1). Without collective enhancement, the maximum probability that the read photon would be scattered into the cavity was only 7.3×10^{-4}, set by the cavity cooperativity parameter, and was nearly three orders of magnitude lower than the observed value of 0.57(9).

To first verify that the light emitted in one polarization was correlated in time with the light in the other polarization, we measured second-order correlation functions $g_{wr}(\tau)|_T$. These are simply the measured coincidence count rate between the detectors D1 and D2 normalized by the rate one would expect for two completely uncorrelated beams of the same average intensities. The label T specifies the size of the coincidence windows (and will hereafter be made implicit), and τ specifies a time offset between the write and read windows. At fixed $T = 8$ ns (Fig. 2, inset), the time-resolved cross-correlation has peak coincidence rates 100(10) times as high as those for uncorrelated beams.

To normalize out possible classical contributions to the cross-correlation data $g_{wr}(20$ ns) of Fig. 2, we also accurately measured the auto-

correlations $g_{ww}(0)$ and $g_{rr}(0)$ using two detectors for each of the write and read beams. For a bin size $T = 60$ ns, the normalized cross-correlation is $G = (g_{wr})^2/(g_{ww}g_{rr}) = 760^{+2100}_{-320}$, representing a large violation of the Cauchy-Schwarz inequality $G \leq 1$ that purely classically correlated beams must satisfy (21).

To assess the usefulness of the system as a source of single photons heralded by the detection of a write photon, we examined two relevant quantities: (i) the recovery efficiency, defined as the probability of generating a read photon conditioned on having detected a write photon; and (ii) the degree to which two–read photon events are suppressed below that of a Poisson distribution with the same average intensity.

A lower bound on the read recovery efficiency R is obtained from the measured detection losses q_r, combined with the measured

probability of detecting a read photon given the detection of a write photon R_{det}^{cond}. The inset to Fig. 3 shows the conditional detection probability versus bin size. The integrated conditional detection probability $R_{det}^{cond} = 0.031(2)$ is estimated from the $T = 0$ intercept of a linear fit to the data at large bin size T. The read photon detection efficiency $q_r = 0.053(8)$ includes contributions from cavity mirror losses (0.45), fiber coupling (0.75), and detector quantum efficiency (0.40). Extrapolated to just outside the cavity output mirror, the recovery efficiency is $R_{cav}^{cond} = 0.26(4)$. The physical recovery efficiency for a cavity of the same linewidth, but with losses completely dominated by transmission of one of the two mirrors, is $R^{cond} = R_{det}^{cond}/q_r = 0.57(9)$. Given the low-finesse $F = 250$ of the present cavity, this ideal regime could be easily achieved with current technologies.
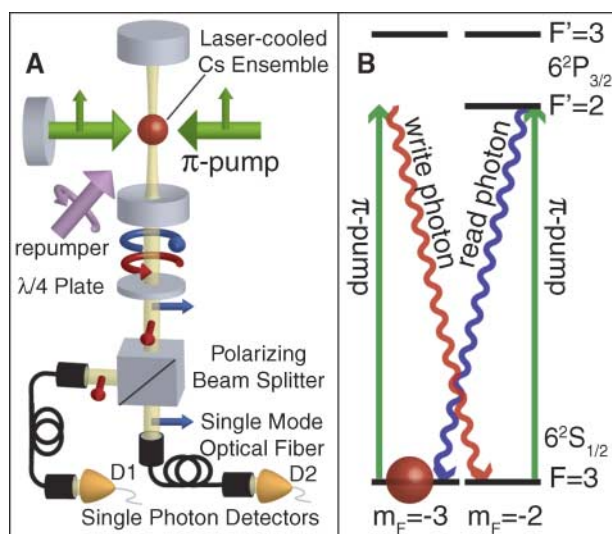
Fig. 1. (A) Experimental setup and **(B)** quantum states used for photon-pair generation. The tuning of the π-pump laser is chosen so that the rate of write photon scattering into the cavity is suppressed by a large detuning from resonance with any excited state, whereas the collectively stimulated generation of a read photon in the cavity proceeds rapidly via resonant coupling. This ensures that the time separation between subsequent pairs exceeds the time separation of the write and read photons within a pair—leading to large cross-correlations between the photon polarizations. The pump and emitted-photon polarizations are denoted by the smaller arrows. The π-pump in combination with a repumper (tuned to the ground $F = 4$ to excited $F' = 4$ transition) optically pumps ~95% of the atomic population into $|F = 3, m_F = -3\rangle$.
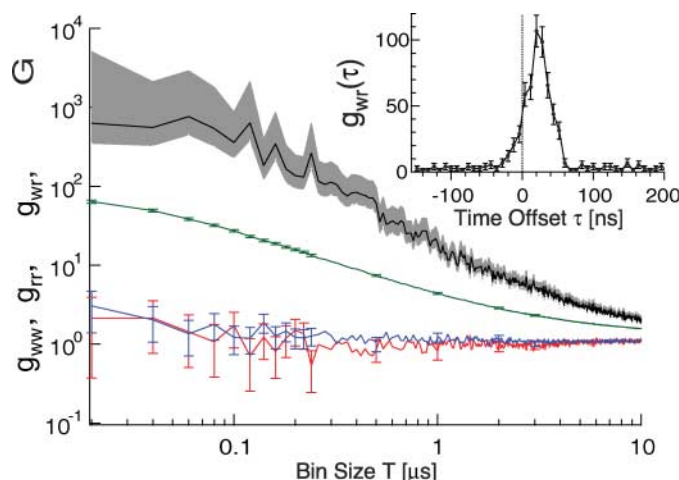
Fig. 2. Nonclassical photon-pair generation. The measured violation of the Cauchy-Schwarz inequality $G = [g_{wr}(\tau)]^2/[g_{ww}(0)g_{rr}(0)] \leq 1$ versus bin size T (black curve with 68% confidence interval), indicating large nonclassical correlations between the write and read photon beams. The inequality simply states that a cross-correlation $g_{wr}(20$ ns) (green) arising from classical sources (i.e., pump-intensity fluctua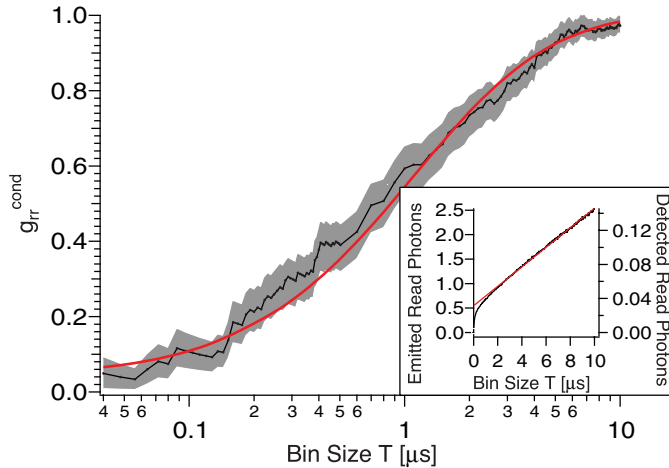tions) must also manifest itself in the measured autocorrelations $g_{ww}(0)$ (red) and $g_{rr}(0)$ (blue). **(Inset)** A time-resolved cross-correlation function $g_{wr}(\tau)$ is shown with a peak value of 100(10).

The conditional suppression of two-photon events was measured using one detector to herald the arrival of a write photon at time t and two detectors to measure the autocorrelation R_{rr}^{cond} of the subset of the read photons that fall within a time bin of size $\pm T/2$ centered at $t + \tau$. With $\tau = 20$ ns, the conditional autocorrelation starts near unity (no suppression) at large bin sizes T (Fig. 3) due to backgrounds not correlated with the registered write photon, and it decreases monotonically until the bin
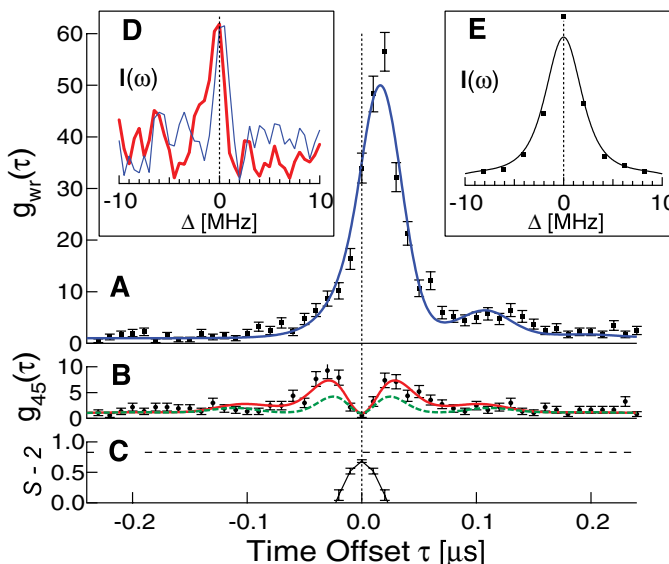
size becomes comparable to the read photon emission time near $T \sim 100$ ns. The largest measured suppression of two-photon events $R_{rr}^{cond} = 0.03(3)$ occurs at $T = 60$ ns.

A conditional single-photon source can only suppress two-photon events to the fundamental limit $R_{rr}^{cond} = \varepsilon_w g_{ww}$ associated with the random emission of two pairs of photons within the same time bin T. In the ideal case, the autocorrelation of the write photons is $g_{ww} = 2$. The write photon generation probability ε_w can be

extracted from the measured write photon detection probability ε^{det} via $\varepsilon_w = \varepsilon_w^{det}/q_w = 0.013(2)$ at $T = 60$ ns, thus predicting the fundamental limit for a conditional photon source at this pair-generation rate of $R_{rr}^{cond} \geq 0.026(3)$. The agreement with the measured value $R_{rr}^{cond} = 0.03(3)$ indicates that spurious background counts are not a serious limitation to the performance of the single-photon source at the present photon-generation rate.

The identicalness of the write and read photons was examined via two-photon interference at the polarizing beam splitter (Fig. 1A) (16–19). This was accomplished by analyzing the write and read photons in a polarization basis rotated by 45° with respect to the usual basis used to deterministically separate the photons. Neglecting interference between the two photons, one expects that in half the cases, the photons register a coincidence count on opposite detectors. However, if the write and read photons perfectly overlap in time and frequency, there is a complete destructive interference for the probability of a coincidence count [a so-called Hong-Ou-Mandel interference (16)]. The fractional reduction of the coincidence count rate below ½ of its original value is a direct measure of the degree of indistinguishability of the photons.

Fig. 3. Performance of the conditional (heralded) single-photon source. The fractional suppression of two-photon events g_{rr}^{cond} and (**inset**) the fractional probability of generating a read photon given the detection of a write photon are both shown versus bin size T. At large bin sizes, read photons generated by other write photons drive the conditional autocorrelation toward the classical limit of unity. As the bin size is reduced, the autocorrelation becomes highly nonclassical ($g_{rr}^{cond} < 1$). As was done for the correlation data in Fig. 2, the average estimate (not maximum-likelihood estimate) is used to avoid underestimating g_{rr}^{cond} and the 68% confidence interval (gray band) at small numbers of counts. The right and left axis of the inset show, respectively, the probabilities conditioned on the detection of a write photon for detection of a read photon (right) and the extrapolated generation of a read photon for a cavity with no mirror losses (left), 57(9)%, extrapolated to $T = 0$. The red curve in (A) is an independent prediction of g_{rr}^{cond} from combining measured background rates with the measured time dependence of the recovery efficiency.

Figure 4 shows the measured coincidence rate expressed as a cross-correlation between detectors D_1 and D_2, when the write and read photons are polarization separated $g_{wr}(\tau)$ (Fig. 4A) and are allowed to interfere $g_{45}(\tau)$ (Fig. 4B). The destructive interference is most pronounced near $\tau = 0$, and it decreases as $|\tau|$ increases because the finite time separation allows one to infer with increasing reliability which detection event corresponds to the write photon and which to the read photon. For data sets at larger π-pump intensities for which the read photons are emitted more promptly, we observe suppressions of the two-photon coincidence rate below ½ by as much as 90(20)% integrated over $T = 5$ μs, indicating that the photons can be made nearly identical.

As a model of the expected two-photon interference for the data of Fig. 4B, we assume that the photons differ by at most a fixed frequency offset $\Delta\omega$ (19). The quantum probabilities C_{wr} and C_{45} that a given photon pair will register as a coincidence event at time separation τ are related by $C_{45}(\tau) = \frac{1}{4}[C_{wr}(\tau) + C_{wr}(-\tau) - 2\sqrt{C_{wr}(\tau)C_{wr}(-\tau)}\cos(2\Delta\omega\tau)]$. Two predictions of $g_{wr}(\tau)$ are obtained from the measured $g_{wr}(\tau)$ and assuming $\Delta\omega/2\pi = 0$ and 2.5 MHz (Fig. 4B). The second prediction accurately describes the observed data, indicating that we are observing a quantum beat between the photons. However, the frequency difference is somewhat larger than the measured Zeeman and calculated light shifts that might give rise to $\Delta\omega \neq 0$.

The two-photon interference results above can be directly mapped onto a *gedanken* version

Fig. 4. Measures of identicalness and photon frequency bandwidths. (**A**) The time-resolved cross-correlation function $g_{wr}(\tau)$ and (**B**) the same function $g_{45}(\tau)$ measured in a polarization basis rotated by 45°. In the 45° basis, coincidence events are suppressed by two-photon interference resulting from the near indistinguishability of the photons. Assuming the photons have identical frequencies, the quantity $g_{45}(\tau)$ can be predicted directly from $g_{wr}(\tau)$ [green dashed curve in (B)]. The prediction is more accurate if a photon frequency difference $\Delta\omega/2\pi = 2.5$ MHz is assumed [red curve in (B)]. (**C**) The predicted violation of a Bell's inequality $S - 2 < 0$ if the photon pairs were used to produce polarization-entangled photons. The dashed line is the maximum possible violation. (**D**) The frequency bandwidths of the write (red) and read (blue) photons are determined to be 1.1(2) MHz from the displayed heterodyne beat notes. For comparison, (**E**) shows the square of the Fourier transform of $\sqrt{g_{wr}(\tau) - 1}$ taken at different parameters, indicating that the photon bandwidths are nearly transform limited.

of the experiments in (*26–29*), wherein polarization entanglement is generated via post selection (see supporting online text and Fig. 4C). The mapping is performed assuming that quantum mechanics is correct (*1, 27–29*). At $\tau = 0$, the predicted CHSH Bell's parameter is $S = 2.68(2)$, a violation of the Bell's inequality $|S| \leq 2$. The predicted violation is not closer to the theoretical maximum $S_{max} = 2\sqrt{2} \approx 2.828$ (dashed line of Fig. 4C), largely due to backgrounds set by the two-photon generation rate.

The frequency bandwidths of the write and read photons are 1.1(2) MHz, making them ideal for interacting with narrowband systems such as atoms, molecules, and optical cavities. By separately heterodyning the write and read photons with laser light derived from the π-pump laser (measured linewidth of 50 kHz), we obtained the power spectral density of the photons from the Fourier transform of the measured second-order autocorrelation function (Fig. 4D). The photons are nearly Fourier-transform limited, as can be seen from the 2-MHz full width at half-maximum power spectrum (Fig. 4E) of the measured cross-correlation function $g_{wr}(\tau)$ taken at slightly different parameters.

These measurements show that pairs of nearly identical photons are generated at an approximate rate of 5×10^4 pairs/s into a single Gaussian transverse mode. The spectral brightness of 5×10^4 pairs/s per MHz^{-1} is ~10^3 times as bright as the best sources based on

parametric downconversion with nonlinear crystals (*8*). The system can operate very near fundamental limits on recovery efficiency, photon bandwidth, and two-photon suppression for a conditional single-photon source. In addition, identical photon pairs are necessary for certain quantum information protocols such as quantum computation with linear optics (*3*). The identical photon pairs also have potential applications for sub-shotnoise spectroscopy of atomic ensembles.

References and Notes

1. A. Aspect, P. Grangier, G. Roger, *Phys. Rev. Lett.* **49**, 91 (1982).
2. L.-M. Duan, M. D. Lukin, J. I. Cirac, P. Zoller, *Nature* **414**, 413 (2001).
3. E. Knill, R. Laflamme, G. Milburn, *Nature* **409**, 46 (2001).
4. Q. A. Turchette, C. J. Hood, W. Lange, H. Mabuchi, H. J. Kimble, *Phys. Rev. Lett.* **75**, 4710 (1995).
5. D. F. Phillips, A. Fleischhauer, A. Mair, R. L. Walsworth, M. D. Lukin, *Phys. Rev. Lett.* **86**, 783 (2001).
6. A. André, L.-M. Duan, M. D. Lukin, *Phys. Rev. Lett.* **88**, 243602 (2002).
7. B. Julsgaard, A. Kozhekin, E. S. Polzik, *Nature* **413**, 400 (2001).
8. F. Konig, E. J. Mason, F. N. C. Wong, M. A. Albota, *Phys. Rev. A.* **71**, 033805 (2005).
9. A. T. Black, J. K. Thompson, V. Vuletić, *Phys. Rev. Lett.* **95**, 133601 (2005).
10. C. H. van der Wal *et al.*, *Science* **301**, 196 (2003).
11. M. D. Eisaman *et al.*, *Phys. Rev. Lett.* **93**, 233602 (2004).
12. A. Kuzmich *et al.*, *Nature* **423**, 731 (2003).
13. C. W. Chou, S. V. Polyakov, A. Kuzmich, H. J. Kimble, *Phys. Rev. Lett.* **92**, 213601 (2004).
14. S. V. Polyakov, C. W. Chou, D. Felinto, H. J. Kimble, *Phys. Rev. Lett.* **93**, 263601 (2004).
15. D. Matsukevich, A. Kuzmich, *Science* **306**, 663 (2004).
16. C. K. Hong, Z. Y. Ou, L. Mandel, *Phys. Rev. Lett.* **59**, 2044 (1987).
17. C. Santori, D. Fattal, J. Vuckovic, G. S. Solomon, Y. Yamamoto, *Nature* **419**, 594 (2002).
18. T. Legero, T. Wilk, M. Hennrich, G. Rempe, A. Kuhn, *Phys. Rev. Lett.* **93**, 070503 (2004).
19. T. Legero, T. Wilk, A. Kuhn, G. Rempe, *Appl. Phys. B* **77**, 797 (2003).
20. V. Balić, D. A. Braje, P. Kolchin, G. Y. Yin, S. E. Harris, *Phys. Rev. Lett.* **94**, 183601 (2005).
21. J. F. Clauser, *Phys. Rev. D* **9**, 853 (1974).
22. M. D. Eisaman *et al.*, *Nature* **438**, 837 (2005).
23. C. W. Chou *et al.*, *Nature* **438**, 828 (2005).
24. T. Chaneliere *et al.*, *Nature* **438**, 833 (2005).
25. D. N. Matsukevich *et al.*, *Phys. Rev. Lett.* **96**, 030405 (2006).
26. J. F. Clauser, M. A. Horne, A. Shimony, R. A. Holt, *Phys. Rev. Lett.* **23**, 880 (1969).
27. Y. H. Shih, C. O. Alley, *Phys. Rev. Lett.* **61**, 2921 (1988).
28. Z. Y. Ou, L. Mandel, *Phys. Rev. Lett.* **61**, 50 (1988).
29. D. Fattal *et al.*, *Phys. Rev. Lett.* **92**, 037903 (2004).
30. This work was supported in parts by grants from NSF, Defense Advanced Research Projects Agency, Army Research Office, and the Sloan Foundation. J.S. acknowledges a National Defense Science and Engineering Graduate Fellowship from the U.S. Department of Defense. H.L. acknowledges a Josephine de Karman Fellowship and a A*STAR (Singapore) Scholarship.

Surface Crystallization in a Liquid AuSi Alloy

Oleg G. Shpyrko,[1,2]* Reinhard Streitel,[1] Venkatachalapathy S. K. Balagurusamy,[1] Alexei Y. Grigoriev,[1] Moshe Deutsch,[3] Benjamin M. Ocko,[4] Mati Meron,[5] Binhua Lin,[5] Peter S. Pershan[1]

X-ray measurements reveal a crystalline monolayer at the surface of the eutectic liquid $Au_{82}Si_{18}$, at temperatures above the alloy's melting point. Surface-induced atomic layering, the hallmark of liquid metals, is also found below the crystalline monolayer. The layering depth, however, is threefold greater than that of all liquid metals studied to date. The crystallinity of the surface monolayer is notable, considering that AuSi does not form stable bulk crystalline phases at any concentration and temperature and that no crystalline surface phase has been detected thus far in any pure liquid metal or nondilute alloy. These results are discussed in relation to recently suggested models of amorphous alloys.

Surface melting—the coexistence of a liquid surface layer with the bulk crystal at temperatures below the bulk melting point T_m—has been observed in a wide range of materials (*1, 2*) and occurs because the entropy of molecules at the free surface is greater than that in the bulk because of the reduced number of their near neighbors. The opposite effect, surface freezing, where a crystalline surface layer coexists with its molten bulk, is much rarer. Surface freezing has been observed, however, in complex liquids composed of high-anisotropy molecules, such as molten unary or

binary alkanes and their derivatives (*3*), and in liquid crystals (*4*). Theory assigns the occurrence of this effect to the highly anisotropic shape of the molecules and to their lengths being greater than the interfacial width (*5*).

Freezing of the surface-segregated component into a two-dimensional (2D) solid layer has also been reported recently in the very dilute binary metallic alloys $Ga_{99.948}Pb_{0.052}$ (*6*) and $Ga_{99.986}Tl_{0.014}$ (*7*). A different ordering effect, surface-induced layering consisting of stratified layers (Fig. 1) near the vapor interface (*8, 9*), has been observed in all liquid metals

and alloys studied to date. The decay of the layering order with depth is exponential and has a range equal to the bulk liquid correlation length (two to three atomic diameters). No surface-parallel ordering was found within these layers in any elemental liquid metal. Similar layering, along with epitaxially induced surface-parallel order, has also been observed in both metallic and nonmetallic liquids near solid/liquid interfaces (*10–12*).

We present evidence for surface crystallization and enhanced surface layering in the liquid $Au_{82}Si_{18}$ eutectic alloy of a type unlike that previously reported for any liquid metal or alloy. A surface monolayer that exhibits lateral long-range crystalline order was found above the eutectic temperature $T_e = 359°C$. Beneath this monolayer, seven to eight layers occur that are liquid in the lateral direction but well defined in the normal direction. The crystalline surface monolayer and the enhancement of the

[1]Department of Physics and Division of Engineering and Applied Sciences, Harvard University, Cambridge, MA 02138, USA. [2]Center for Nanoscale Materials, Argonne National Laboratory, Argonne, IL 60439, USA. [3]Department of Physics, Bar-Ilan University, Ramat-Gan 52900, Israel. [4]Condensed Matter Physics and Materials Science Department, Brookhaven National Laboratory, Upton, NY 11973, USA. [5]Center for Advanced Radiation Sources, University of Chicago, Chicago, IL 60637, USA.

*To whom correspondence should be addressed. E-mail: oshpyrko@anl.gov